Numerical analysis of viscoelastic pipe with variable fractional order model based on shifted Legendre polynomials algorithm

Suhua Jin[1] | Yiming Chen*[1,2] | Yuanhui Wang[1]

[1]School of Science, Yanshan University, Qinhuangdao 066004, China

[2]LE STUDIUM RESEARCH Professor, Loire Valley Institute for Advanced Studies, 45000 Orléans, France

Correspondence
Yiming Chen, School of Science, Yanshan University, Qinhuangdao 066004, China
LE STUDIUM RESEARCH Professor, Loire Valley Institute for Advanced Studies, 45000 Orléans, France
Email: chenym@ysu.edu.cn

Summary

In this paper, an valid numerical algorithm is presented to solve variable fractional viscoelastic pipes conveying pulsating fluid in the time domain and analyze dynamically the vortex-induced vibration of the pipes. Firstly, Coimbra variable fractional derivative operators are introduced. Meanwhile, using Hamilton's principle and a nonlinear variable fractional order model, the governing system of equations is established. The unknown functions of the system of equations are approximated with shifted Legendre polynomials. Then, convergence analysis and numerical example investigate the effectiveness and accuracy of the proposed algorithm. Finally, the influences of different parameters on the dynamic response of the viscoelastic pipe are studied. The influencing factors and their ranges of the transient and long-term chaotic states of the pipe are analyzed. In addition, the proposed algorithm shows enormous potentials for solving the dynamics problems of viscoelastic pipes with the variable fractional order models.

KEYWORDS:
Nonlinear variable fractional order model , Viscoelastic pipe , Shifted Legendre polynomials algorithm , Numerical solution , Vortex-induced vibration

1 | INTRODUCTION

Viscoelastic materials are often used to vibrating structures for improving damping capability of the structures. The damping capability of the structure highly depends on the properties of the viscoelastic materials within the damped structure [1]. Therefore, it is of great significance to study the mechanical properties of viscoelastic materials. In recent years, many integer order mathematical models have been developed to describe the viscoelasticity of materials in practical applications. Mohammad et al. [2] used artificial neural network and Maxwell model to predict the viscoelastic behavior of pomegranate. Yan et al. [3] selected Kelvin-Voight model to represent the character of viscoelastic interfaces. Because the fractional order model is more freedom degrees and accurate than the integer order model. The fractional order model has been widely used in many fields of science and engineering [4]. As a result, the fractional order model is applied to describe the viscoelastic behavior of materials. Yu et al. [5] applied the fractional order Kelvin model as the constitution model to study the dynamic displacement varying with position and time. Martin [6] used fractional order Zenner model to investigate the dynamic analysis of a viscoelastic nanobeam. It was analyzed the effect of the fractional derivative on the nanobeam. Yin et al. [7] used fractional order Maxwell model to study oscillating flow of a viscoelastic fluid in a pipe. However, the variable fractional order model is more suitable than the fractional order model for variable memory and can better simulate the viscoelastic constitutive relations [8]. Li et al. [9] studied a numerical algorithm to simulate the variable fractional order of the shape-memory polymer owing viscoelastic property

and compare with the fractional order. For accurately modelling the viscoelastic constitution relation, a variable fractional order model was also proposed in [10]. The compression deformation of amorphous glassy polymers in viscoelastic region with the variable fractional order model was investigated. Cai et al. [11] adopted a variable fractional order constitutive model to characterize tensile behaviors of sintered nano-silver paste at different strain rates and ambient temperatures. Meng et al. [12] provided a novel approach of variable fractional derivative model of viscoelasticity to describe the strain hardening behavior of amorphous glassy polymers. These results all demonstrated the variable fractional order model can better simulate the viscoelastic constitutive relationship.

Vortex-induced vibration encountered usually with pipes conveying fluid is an important phenomenon of fluid-structure interaction. In the application of ocean engineering, the vortex-induced vibration of pipe is a factor that must be considered. As vortex-induced vibration occurring, the external fluid applies lift forces and oscillatory drag on the pipe, which causes the pipe oscillate or move rigidly. In addition, the internal fluid velocity and density, external excitation and other factors also affect the dynamic response of the pipe. The pipe will enter a chaotic or stable state depending on whether these factors reach a critical value. This may lead to fatigue damage of structures such as risers, mooring lines and pipes [13].

In order to avoid the loss caused by fatigue failure of pipes, many scholars begin to analyze vortex-induced vibration of pipes. Dai et al. [14] examined the vortex-induced vibration of the pipe with the internal fluid velocity varying from the subcritical to the supercritical regions. A mount of dynamical behaviors, such as periodic and chaotic motions were occurred by the time of the internal fluid velocity varying in the supercritical regions. Duan et al. [15] studied vortex-induced vibration of a flexible fluid-conveying pipe for internal and cross flow. With different internal and cross flow velocities, a flexible riser appeared the jumping phenomenon, quasi-periodic and chaotic motions. Xie et al. [16] investigated a flexible pipe conveying variable density internal fluid and undergoing vortex-induced vibrations. Dynamic response of the pipe would become more obvious for the fluctuation amplitude of the internal fluid density varying. Dai et al. [17] researched vortex-induced vibration of the pipe conveying pulsating fluid. Then the consequent demonstrated the peak response amplitude of the pipe can be adjusted by the frequency of the internal pulsating fluid. Yang et al. [18] predicted the dynamic response of the flexible pipe conveying fluid for different internal and cross flow velocity. Zhang et al. [19] noticed the effect of harmonic tension on fluid-conveying pipes undergoing vortex-induced vibration. Displacements and stresses were increasing and the resonance regions became wider with harmonic tension amplitude increasing. Although the above studies discussed the effects of time, internal and external fluid velocity, fluid density and other factors on the pipe, none of the pipe materials were considered. Studies [20][21] have shown that viscoelastic materials have a significant effect on weakening vibration response to hydraulic and structural transients. Viscoelastic materials greatly improve the stability of the vortex-induced vibration of the pipe. Yang et al. [22] selected Kelvin-Voight model to study the impacts of the viscoelastic coefficients on displacements, stresses, modal variation and phase portraits. It demonstrated that appropriate viscoelastic coefficients were very important to effectively suppress the maximum displacements and stresses. However, there is little research on vortex-induced vibration of viscoelastic pipes conveying fluid. In order to predict the dynamic response which contains stable states and chaotic motions conditions, vortex-induced vibration of viscoelastic pipes is researched in this paper.

Dynamic analysis needs accurate and effective algorithm. The governing equation of pipe should be established by using the variable fractional order model. Moreover, the governing equation is a class of nonlinear variable fractional order differential system of equations containing analytic functions. Many scholars have studied fractional order differential equations and systems of equations before. Qu et al. [23] proposed neural network method to solve the fractional heat conduction equation and the fractional wave equation. Ramezani [24] solved nonlinear multi-term time fractional differential equation based on collocation method via fractional B-spline. Ansari et al. [25] used the fractional exponential operators to solve system of partial fractional differential equations. The validity of this operator in obtaining the formal solution of diffusion equations was discussed. Recently, the numerical solutions of the variable fractional order differential equations and system of equations have been further studied. Chen et al. [26] proposed a numerical method to estimate a variable fractional order of unknown signal equation in noisy environment. El-Sayed et al. [27] introduced a method of solving multiterm variable-order fractional differential equations. The basic problem was reduced to a set of algebraic equations by using constructed shifted Legendre polynomials matrices and configuration techniques. A Bernstein polynomial numerical method for solving a class of variable fractional order linear cable equations was proposed in [28]. The two-dimensional variable fractional order time advection-diffusion equations were solved by a meshless method [29] and a radial basis function-based differential quadrature method [30]. For variable fractional order differential system of equations, Faghih and Mokhtary [31] were concerned with a new fractional Jacobi collocation method for solving a system of multi-order fractional differential equations with variable coefficients. Heydari et al. [32] generalized a coupled system of reaction-advection-diffusion equations to a variable fractional order one. The orthogonal shifted

discrete Legendre polynomials were introduced to solve obtained system of equations. However, there are few studies on the numerical solutions of viscoelastic pipe of nonlinear variable fractional order differential governing system of equations.

Based on these reasons, the shifted Legendre polynomials algorithm is proposed to solve the nonlinear variable fractional order differential governing system of equations of the pipe. This algorithm utilizes shifted Legendre polynomials as basis functions to approximate the analytic function, and uses the product of the differential operator matrices and the basis function to represent the derivative of the analytic function. The algorithm provides algorithm support for the variable fractional order model and viscoelastic materials.

The structure of this article is as follows: In Section 2, the variable fractional order model is selected as the constitutive model to derive the governing system of equations of the pipe. In Section 3, the shifted Legendre polynomials algorithm is proposed to obtain the numerical solution of the governing system of equations. In Section 4, convergence analysis is presented. In Section 5, three numerical examples are given to verify the accuracy of the proposed algorithm. In Section 6, the dynamics effects of various parameters on pipe are studied and the conditions of stable states and chaotic motions are discussed. Finally, Section 7, gives the conclusion.

2 | MATHEMATICAL PRELIMINARIES AND ANALYTICAL MODEL

The definitions and properties of the variable fractional calculus operators are introduced, and the governing equations are derived by introducing the variable fractional order model.

Definition 1. The Coimbra variable fractional derivative operator $D_t^{\alpha(x)}$ of order $\alpha(x)$ is defined as [33]

$$D_t^{\alpha(x)} f(x,t) = \frac{1}{\Gamma(1-\alpha(x))} \int_{0^+}^{t} (t-\tau)^{-\alpha(x)} \frac{\partial f(x,\tau)}{\partial \tau} d\tau + \frac{\left(f\left(x,0^+\right) - f\left(x,0^-\right)\right) t^{-\alpha(x)}}{\Gamma(1-\alpha(x))} \tag{1}$$

where $t \geq 0$, $0 < \alpha(x) \leq 1$, $\alpha(x)$ is variable fractional order, $f(t)$ is continuous over interval $(0,+\infty)$ and is integrable over any subinterval of $[0,+\infty)$, $\Gamma(\cdot)$ denotes the Euler Gamma function.

Definition 2. For two-dimensional variable fractional order $\alpha(x,t)$, the Coimbra variable fractional derivative operators are defined as follows [33]:

$$D_t^{\alpha(x,t)} f(x,t) = \frac{1}{\Gamma(1-\alpha(x,t))} \int_{0^+}^{t} (t-\tau)^{-\alpha(x,t)} \frac{\partial f(x,\tau)}{\partial \tau} d\tau + \frac{\left(f\left(x,t_{0^+}\right) - f\left(x,t_{0^-}\right)\right) t^{-\alpha(x,t)}}{\Gamma(1-\alpha(x,t))} \tag{2}$$

In the case of $f\left(x,t_{0^+}\right) = f\left(x,t_{0^-}\right)$ in the Definition 2, the operator would be correspondent to the well-known Caputo fractional operator. Therefore, based on the definition of the variable fractional derivative in the Caputo sense, the following formula can be expressed as:

$$D_t^{\alpha(x,t)} t^m = \begin{cases} \frac{\Gamma(m+1)}{\Gamma(m+1-\alpha(x,t))} t^{m-\alpha(x,t)}, & \alpha(x,t) - m \notin \mathbb{N} \\ 0, & else. \end{cases} \tag{3}$$

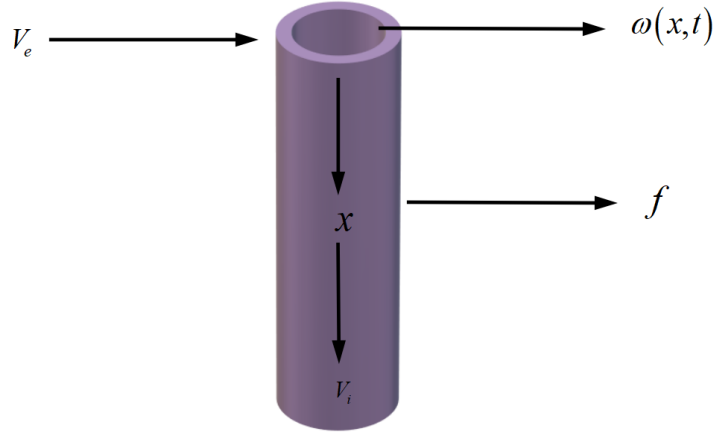This property facilitates the algorithm proposed later.

FIGURE 1 The geometric figure of viscoelastic pipes conveying fluid under external fluid and load excitation.

Vortex-induced vibration of viscoelastic pipes conveying fluid is studied in this paper. It is simply supported at both ends as shown in Fig. 1 . The governing system of equations can be derived by a variable fractional order constitutive model [34] and Hamilton's principle without considering gravity effects. Also, it is formulated as:

$$
\begin{cases}
m\dfrac{\partial^2 w}{\partial t^2} + 2m_f V_i \dfrac{\partial^2 w}{\partial x \partial t} + \left[m_f V_i^2 + m_f \dfrac{\partial V_i}{\partial t}(L-x) - P_0 \right] \dfrac{\partial^2 w}{\partial x^2} \\[2mm]
\qquad + (C_s + \dfrac{1}{2} C_D \rho_0 D V_e) \dfrac{\partial w}{\partial t} + EI\theta^\alpha \dfrac{\partial^{4+\alpha} w}{\partial x^4 \partial t^\alpha} = \dfrac{1}{4} C_{L_0} \rho_0 D V_e^2 q + f_e \\[2mm]
\dfrac{\partial^2 q}{\partial t^2} + \lambda w_s (q^2 - 1)\dfrac{\partial q}{\partial t} + w_s^2 q = \dfrac{A_w}{D}\dfrac{\partial^2 w}{\partial t^2} \\[2mm]
\alpha = \begin{cases} \alpha_0 - \alpha_k (\dfrac{D}{2}\dfrac{\partial^2 w}{\partial x^2} - \alpha_b), & \dfrac{\partial^2 w}{\partial x^2} \geq \dfrac{2\alpha_b}{D} \\[2mm] \alpha_0, & 0 \leq \dfrac{\partial^2 w}{\partial x^2} < \dfrac{2\alpha_b}{D} \end{cases}
\end{cases}
\tag{4}
$$

The boundary conditions are

$$
w(0,t) = 0, \quad w(L,t) = 0, \quad \frac{\partial w(0,t)}{\partial x} = 0, \quad \frac{\partial w(L,t)}{\partial x} = 0.
\tag{5}
$$

TABLE 1 The physical quantities in governing system of equations (4)

Physical quantity	Symbol	Dimension	Physical quantity	Symbol	Dimension
Mass per unit length of the pipe	m	$\mathrm{kg \cdot m^{-1}}$	Lift coefficient in the transverse direction	C_{L_0}	1
Mass per unit length of internal and additional external fluid	m	$\mathrm{kg \cdot m^{-1}}$	Density of external fluid	ρ_0	$\mathrm{kg \cdot m^{-3}}$
Mass per unit length of internal fluid	m_f	$\mathrm{kg \cdot m^{-1}}$	Constitution model parameter	E	Pa
Transverse displacement of the pipe	w	m	Area moment of inertia	I	$\mathrm{m^4}$
Position	x	m	Constitution model parameter	θ	1
Time	t	s	Constitution model parameter	α	1
Length of the pipe	L	m	Reduced lift coefficient	q	1
Outer diameter of the pipe	D	m	Constant parameter	λ	1
Internal fluid velocity	V_i	$\mathrm{m \cdot s^{-1}}$	Vortex-shedding frequency	w_s	Hz
External fluid velocity	V_e	$\mathrm{m \cdot s^{-1}}$	Constant parameter	A_w	1
Internal damping coefficient	C_s	$\mathrm{N \cdot s \cdot m^{-2}}$	Force excitation	f_e	$\mathrm{N \cdot m^{-1}}$
Hydrodynamic damping coefficient in the transverse direction	C_D	1	Tensional force	P_0	N

The physical quantities in governing system of equations (4) are interpreted as shown in Table 1 . Moreover, w and q are the analytical functions of Eq.(4).

It is noted that C_D, C_{L_0}, λ, A_w always respectively values 1.2, 0.3, 0.3, 12 and the specific derivation process can be seen in A.

The variable fractional order α is a piecewise function which satisfies $0 < \alpha < 1$. α values a constant α_0 when strain of the pipe is less than the threshold, and a function $\alpha_0 - \alpha_k(\frac{D}{2}\frac{\partial^2 w}{\partial x^2} - \alpha_b)$ when strain of the pipe is equal to or more than the threshold. Here the strain and threshold are respectively as $\frac{D}{2}\frac{\partial^2 w}{\partial x^2}$ and α_b. In other words, the variable fractional order α is a constant at the time of small deformation and a function containing an unknown analytical solution at the time of large deformation.

3 | SHIFTED LEGENDRE POLYNOMIALS ALGORITHM

In this part, the shifted Legendre polynomials algorithm is presented to solve numerically this class of nonlinear variable fractional order differential system of equations, which is a piecewise function containing analytic functions. Moreover, the following section is the specific process of this algorithm.

3.1 | Shifted Legendre polynomials

The shifted Legendre polynomial of degree n in $[0, 1]$ [35] is defined as

$$u_{n,i}(x) = \sum_{i=0}^{n} (-1)^{n+i} \frac{\Gamma(n+i+1)}{\Gamma(n-i+1)(\Gamma(i+1))^2} x^i \tag{6}$$

where $i = 0, 1, \cdots, n$, $x \in [0, 1]$. Then a series of shifted Legendre polynomials matrix $\varphi(x)$ can be written as

$$\varphi(x) = \left[u_{n,0}(x), u_{n,1}(x), \cdots, u_{n,n}(x)\right] = H Z(x) \tag{7}$$

where $Z(x) = [1, x, \cdots, x^n]^T$,

$$H = [h_{ij}]_{i,j=0}^{n}, \quad h_{ij} = \begin{cases} 0, & i < j \\ (-1)^{i+j} \dfrac{\Gamma(i+j+1)}{\Gamma(i-j+1)(\Gamma(j+1))^2}, & i \geq j. \end{cases}$$

For expanding the range of x, the shifted Legendre polynomial of degree n in $[0, L]$ is formulated as:

$$p_{n,i}(x) = \sum_{i=0}^{n} (-1)^{n+i} \frac{\Gamma(n+i+1)}{\Gamma(n-i+1)(\Gamma(i+1))^2} \left(\frac{1}{L}\right)^i x^i \tag{8}$$

where $i = 0, 1, \cdots, n$, $x \in [0, L]$. Then a series of shifted Legendre polynomials matrix $\Psi(x)$ can be written as

$$\Psi(x) = [p_{n,0}(x), p_{n,1}(x), \cdots, p_{n,n}(x)]^T = R Z(x) \tag{9}$$

where

$$R = [r_{ij}]_{i,j=0}^{n}, \quad r_{ij} = \begin{cases} 0, & i \neq j \\ (-1)^{n+i} \frac{\Gamma(i+j+1)}{\Gamma(i-j+1)(\Gamma(i+1))^2} L^{-i}, & i = j. \end{cases}$$

Similarly, a series of shifted Legendre polynomials matrix $\Phi(t)$ in $[0, S]$ can be defined as

$$\Phi(t) = \left[p_{n,0}(t), p_{n,1}(t), \cdots, p_{n,n}(t)\right] = M Z(t) \tag{10}$$

where

$$M = [m_{ij}]_{i,j=0}^{n}, \quad m_{ij} = \begin{cases} 0, & i \neq j \\ (-1)^{n+i} \frac{\Gamma(i+j+1)}{\Gamma(i-j+1)(\Gamma(i+1))^2} S^{-i}, & i = j. \end{cases}$$

3.2 | Function approximation

A continuous function $T(x)$ in the domain $[0, L]$ can be approached with the form of shifted Legendre polynomials as $T(x) = \sum_{i=0}^{\infty} c_i p_{n,i}(x)$, $T(x)$ can be approximated as:

$$T(x) \approx T_n(x) = \sum_{i=0}^{n} c_i p_{n,i}(x) = C^T \Psi(x) \tag{11}$$

where $C^T = [c_0, c_1, \cdots, c_n]$ is an unknown coefficient matrix. Then

$$\langle T(x), \Psi^T(x) \rangle = C^T \langle \Psi(x), \Psi^T(x) \rangle = C^T Q \tag{12}$$

where $Q = \langle \Psi(x), \Psi^T(x) \rangle = [\delta_{ij}]_{i,j=0}^{n}$, $\delta_{ij} = \int_0^L p_{n,i}(x) p_{n,j}(x) dx$, $C^T = \langle T(x), \Psi^T(x) \rangle Q^{-1}$.

Two-variable continuous function $T(x, t) \in L^2[0, L] \times [0, S]$ can be described as:

$$\begin{aligned} T(x, t) &= \sum_{j=0}^{\infty} \left(\sum_{i=0}^{\infty} c_i p_{n,i}(x) \right) k_j p_{n,j}(t) \\ &= \sum_{j=0}^{\infty} \sum_{i=0}^{\infty} c_i k_j p_{n,i}(x) p_{n,j}(t) \\ &= \sum_{j=0}^{\infty} \sum_{i=0}^{\infty} \Omega_{ij} p_{n,i}(x) p_{n,j}(t) \end{aligned} \tag{13}$$

If we consider truncated series in (13), then it can rewritten as:

$$\begin{aligned} T(x, t) &\approx \sum_{j=0}^{n} \sum_{i=0}^{n} \Omega_{ij} p_{n,i}(x) p_{n,j}(t) \\ &= \Omega^T [\Psi(x) \otimes \Phi(t)] \end{aligned} \tag{14}$$

where $\Omega = [\Omega_{00}, \Omega_{01}, \cdots, \Omega_{0n}, \Omega_{10}, \Omega_{11}, \cdots, \Omega_{1n}, \cdots, \Omega_{n0}, \Omega_{n1}, \cdots, \Omega_{nn}]^T$, $\Omega = C \otimes K$, and $\otimes$ is Kronecker product. Thus, $w(x, t)$ and $q(x, t)$ can be noted as:

$$\begin{cases} w(x, t) \approx w_n(x, t) = \Omega_1^T [\Psi(x) \otimes \Phi(t)] \\ q(x, t) \approx q_n(x, t) = \Omega_2^T [\Psi(x) \otimes \Phi(t)] \end{cases} \tag{15}$$

3.3 | Differential operator matrices

In this section, differential operator matrices need to be solved for expressing the derivative function of analytic function. $\Psi(x)$ are a series of polynomials matrices with respect to x, the derivative of $\Psi(x)$ with respect to x is formulated as:

$$\Psi'(x) = (RZ(x))' = R(Z(x))' = RVZ(x) = RVR^{-1}\Psi(x) = B\Psi(x) \tag{16}$$

where $V = [v_{ij}]_{i,j=0}^{n}$, $v_{ij} = \begin{cases} 0, & i \neq j+1 \\ i, & i = j+1. \end{cases}$

$B = RVR^{-1}$ is first order differential operator matrix. Similarly, second order differential operator matrix B^2 can be written as:

$$B^2 = RV^2R^{-1} \tag{17}$$

And so on, m order differential operator matrix B^m can be written as:

$$B^m = RV^m R^{-1} \tag{18}$$

The α order derivative of $\Phi(t)$ with respect to t is formulated as:

$$\frac{d^\alpha \Phi}{dt^\alpha} = B^{\alpha(t)} \Phi(t), \quad \alpha \in (0, 1). \tag{19}$$

Then

$$B^{\alpha(t)} \Phi(t) = B^{\alpha(t)} MZ(t) = M \frac{d^\alpha Z(t)}{dt^\alpha} = MGZ(t) = MGM^{-1}\Phi(t) \tag{20}$$

where $G = [g_{ij}]_{i,j=0}^n$, $\quad g_{ij} = \begin{cases} \frac{\Gamma(i+1)}{\Gamma(i+1-\alpha)} t^{-\alpha}, & i = j, i \geq 1 \\ 0, & otherwise. \end{cases}$ The variable fractional order differential operator matrix $B^{\alpha(t)}$ can be described as:

$$B^{\alpha(t)} = MGM^{-1} \tag{21}$$

Thus, integer-fractional differential term of $w(x,t)$ and $q(x,t)$ can be noted as:

$$\begin{cases} \dfrac{\partial^{m+v} w(x,t)}{\partial x^m \partial t^v} \approx \Omega_1^T \left[(B^m \Psi(x)) \otimes (B^v \Phi(t)) \right] \\[3mm] \dfrac{\partial^{m+\alpha} w(x,t)}{\partial x^m \partial t^\alpha} \approx \Omega_1^T \left[(B^m \Psi(x)) \otimes (B^{\alpha(t)} \Phi(t)) \right] \end{cases} \tag{22}$$

$$\begin{cases} \dfrac{\partial^{m+v} q(x,t)}{\partial x^m \partial t^v} \approx \Omega_2^T \left[(B^m \Psi(x)) \otimes (B^v \Phi(t)) \right] \\[3mm] \dfrac{\partial^{m+\alpha} q(x,t)}{\partial x^m \partial t^\alpha} \approx \Omega_2^T \left[(B^m \Psi(x)) \otimes (B^{\alpha(t)} \Phi(t)) \right] \end{cases} \tag{23}$$

where Ω_1 and Ω_2 are unknown coefficient matrices.

Finally, the governing system of equations (4) will be converted into the following algebraic system of equations:

$$\begin{cases} m\Omega_1^T \left[\Psi(x) \otimes (B^2 \Phi(t)) \right] + 2m_f V_i \Omega_1^T \left[(B\Psi(x)) \otimes (B\Phi(t)) \right] \\[2mm] \quad + \left[m_f V_i^2 + m_f \dfrac{\partial V_i}{\partial t}(L-x) - P_0 \right] \Omega_1^T \left[(B^2 \Psi(x)) \otimes \Phi(t) \right] \\[2mm] \quad + (C_s + \dfrac{1}{2} C_D \rho_0 V_e) \Omega_1^T \left[\Psi(x) \otimes (B\Phi(t)) \right] + EI\theta^\alpha \Omega_1^T \left[(B^4 \Psi(x)) \otimes (B^{\alpha(t)}\Phi(t)) \right] \\[2mm] \quad = \dfrac{1}{4} C_{L_0} \rho_0 D V_e^2 \Omega_2^T \left[\Psi(x) \otimes \Phi(t) \right] + f_e \\[3mm] \Omega_2^T \left[\Psi(x) \otimes (B^2 \Phi(t)) \right] + \lambda w_s \left[\left(\Omega_2^T (\Psi(x) \otimes \Phi(t)) \right)^2 - 1 \right] \Omega_2^T \left[\Psi(x) \otimes (B\Phi(t)) \right] \\[2mm] \quad + w_s^2 \Omega_2^T \left[\Psi(x) \otimes \Phi(t) \right] = \dfrac{A_w}{D} \Omega_1^T \left[\Psi(x) \otimes (B^2 \Phi(t)) \right] \\[3mm] \alpha = \begin{cases} \alpha_0 - \alpha_k \{ \dfrac{D}{2} \Omega_1^T \left[(B^2 \Psi(x)) \otimes \Phi(t) \right] - \alpha_b \}, & \Omega_1^T \left[(B^2 \Psi(x)) \otimes \Phi(t) \right] \geq \dfrac{2\alpha_b}{D} \\[3mm] \alpha_0, & \Omega_1^T \left[(B^2 \Psi(x)) \otimes \Phi(t) \right] < \dfrac{2\alpha_b}{D} \end{cases} \end{cases} \tag{24}$$

where only Ω_1 and Ω_2 are unknown. x and t are discretized to points (x_i, t_j), where $x_i = i\frac{L}{n}$ and $t_j = j\frac{S}{n}$, Ω_1 and Ω_2 are obtained by solving the above algebraic system of equations (24) based on least squares. Solutions $w_n(x,t)$ and $q_n(x,t)$ are obtained by Eq.(15) as the approximation of the exact solutions $w(x,t)$ and $q(x,t)$. Also, solutions $w_n(x,t)$ and $q_n(x,t)$ can be seen as the interpolating polynomial of the exact solutions $w(x,t)$ and $q(x,t)$.

4 | CONVERGENCE ANALYSIS

The aim of this section is to investigate the convergence of the proposed numerical algorithm. For doing this, the Banach space $W = C[0,L] \times C[0,S]$ of all continuous functions on $\Xi = [0,L] \times [0,S]$ is considered with the following norm:

$$||w(x,t)|| = \langle w(x,t), w(x,t) \rangle^{\frac{1}{2}} = (\int_0^S \int_0^L |w(x,t)|^2 dx dt)^{\frac{1}{2}}. \tag{25}$$

Similarly, the norm of continuous function $q(x,t)$ in the Banach space can also be formulated as

$$||q(x,t)|| = \langle q(x,t), q(x,t) \rangle^{\frac{1}{2}} = (\int_0^S \int_0^L |q(x,t)|^2 dx dt)^{\frac{1}{2}}. \tag{26}$$

Theorem 1. Suppose that $w(x, t)$ and $q(x, t)$ are the exact solutions, $w_n(x, t)$ and $q_n(x, t)$ are the approximate solutions obtained by the shifted Legendre polynomials algorithm in the Banach space $W = C[0, L] \times C[0, S]$. Then

$$||w_n(x, t) - w(x, t)|| \leq (LS)^{\frac{1}{2}} \left[A_1 (\frac{L}{n})^{n+1} + A_2 (\frac{S}{n})^{n+1} + A_3 (\frac{(LS)^{\frac{1}{2}}}{n})^{2n+2} \right]$$

(27)

$$||q_n(x, t) - q(x, t)|| \leq (LS)^{\frac{1}{2}} \left[B_1 (\frac{L}{n})^{n+1} + B_2 (\frac{S}{n})^{n+1} + B_3 (\frac{(LS)^{\frac{1}{2}}}{n})^{2n+2} \right]$$

where A_1, A_2, A_3, B_1, B_2 and B_3 are terminate constants.

Proof. $w_n(x, t)$ is the numerical solution obtained as the interpolating polynomial of $w(x, t)$ at points (x_i, t_j) by means of shifted Legendre polynomials algorithm, where $x_i = i\frac{L}{n}$ and $t_j = j\frac{S}{n}$. Then, one can obtain

$$w(x, t) - w_n(x, t) = \frac{\partial^{n+1} w(\varrho, t)}{\partial x^{n+1}} \frac{\prod_{i=0}^{n}(x - x_i)}{(n + 1)!} + \frac{\partial^{n+1} w(x, \zeta)}{\partial t^{n+1}} \frac{\prod_{j=0}^{n}(t - t_j)}{(n + 1)!}$$

(28)

$$- \frac{\partial^{2n+2} w(\varrho', \zeta')}{\partial x^{n+1} \partial t^{n+1}} \frac{\prod_{i=0}^{n}(x - x_i) \prod_{j=0}^{n}(t - t_j)}{[(n + 1)!]^2}$$

for $\varrho, \varrho' \in [0, L]$ and $\zeta, \zeta' \in [0, S]$. Thus, we can have

$$|w_n(x, t) - w(x, t)| \leq \max_{(x,t)\in\Xi} \left| \frac{\partial^{n+1} w(x, t)}{\partial x^{n+1}} \right| \frac{\prod_{i=0}^{n} |x - x_i|}{(n + 1)!}$$

$$+ \max_{(x,t)\in\Xi} \left| \frac{\partial^{n+1} w(x, t)}{\partial t^{n+1}} \right| \frac{\prod_{j=0}^{n} |t - t_j|}{(n + 1)!}$$

(29)

$$+ \max_{(x,t)\in\Xi} \left| \frac{\partial^{2n+2} w(x, t)}{\partial x^{n+1} \partial t^{n+1}} \right| \frac{\prod_{i=0}^{n} |x - x_i| \prod_{j=0}^{n} |t - t_j|}{[(n + 1)!]^2}.$$

To find the bounds on $\prod_{i=0}^{n} |x - x_i|$ and $\prod_{j=0}^{n} |t - t_j|$, defining the variables $x = \vartheta \frac{L}{n}$ and $t = \vartheta' \frac{S}{n}$, it gives that

$$\prod_{i=0}^{n} |x - x_i| = (\frac{L}{n})^{n+1} \prod_{i=0}^{n} |\vartheta - i|$$

$$\prod_{j=0}^{n} |t - t_j| = (\frac{S}{n})^{n+1} \prod_{j=0}^{n} |\vartheta' - j|.$$

By choosing the integers N_1 and N_2 which are less than n, we have $\vartheta \in (N_1, N_1 + 1)$ and $\vartheta' \in (N_2, N_2 + 1)$, therefore

$$\prod_{i=0}^{n} |\vartheta - i| = |(\vartheta - N_1)(\vartheta - N_1 - 1)| \prod_{i=0}^{N_1-1} |\vartheta - i| \prod_{i=N_1+2}^{n} |\vartheta - i|$$

(30)

$$\prod_{j=0}^{n} |\vartheta' - j| = |(\vartheta' - N_2)(\vartheta' - N_2 - 1)| \prod_{i=0}^{N_2-1} |\vartheta' - j| \prod_{j=N_2+2}^{n} |\vartheta' - j|.$$

Note that $|(\vartheta - N_1)(\vartheta - N_1 - 1)|$ and $|(\vartheta' - N_2)(\vartheta' - N_2 - 1)|$ have maximum when ϑ and ϑ' values at points $N_1 + \frac{1}{2}$ and $N_2 + \frac{1}{2}$, respectively, thus

$$|(\vartheta - N_1)(\vartheta - N_1 - 1)| \leq \frac{1}{4}$$

$$|(\vartheta' - N_2)(\vartheta' - N_2 - 1)| \leq \frac{1}{4}.$$

And we can get

$$\prod_{i=0}^{N_1-1} |\vartheta - i| \prod_{i=N_1+2}^{n} |\vartheta - i| \leq \prod_{i=0}^{N_1-1} (N_1 + 1 - i) \prod_{i=N_1+2}^{n} (i - N_1) = (N_1 + 1)!(n - N_1)! \leq (n + 1)!.$$

(31)

and

$$\prod_{i=0}^{N_2-1} |\vartheta' - i| \prod_{i=N_2+2}^{n} |\vartheta' - i| \le \prod_{i=0}^{N_2-1} (N_2 + 1 - i) \prod_{i=N_2+2}^{n} (i - N_2) = (N_2 + 1)!(n - N_2)! \le (n+1)!. \tag{32}$$

Substituting (31)-(32) into (30), it yields

$$\prod_{i=0}^{n} |\vartheta - i| = |(\vartheta - N_1)(\vartheta - N_1 - 1)| \prod_{i=0}^{N_1-1} |\vartheta - i| \prod_{i=N_1+2}^{n} |\vartheta - i| \le \frac{1}{4}(n+1)!. \tag{33}$$

and

$$\prod_{j=0}^{n} |\vartheta' - j| = |(\vartheta' - N_2)(\vartheta' - N_2 - 1)| \prod_{j=0}^{N_2-1} |\vartheta' - j| \prod_{j=N_2+2}^{n} |\vartheta' - j| \le \frac{1}{4}(n+1)!. \tag{34}$$

Therefore, according to (30), (33) and (34), one has

$$\prod_{i=0}^{n} |x - x_i| \le (\frac{L}{n})^{n+1} \frac{1}{4}(n+1)!$$
$$\prod_{j=0}^{n} |t - t_j| \le (\frac{S}{n})^{n+1} \frac{1}{4}(n+1)!.$$

Considering $A_1 = \max_{(x,t) \in \Xi} \frac{1}{4} \left| \frac{\partial^{n+1} w(x,t)}{\partial x^{n+1}} \right|$, $A_2 = \max_{(x,t) \in \Xi} \frac{1}{4} \left| \frac{\partial^{n+1} w(x,t)}{\partial t^{n+1}} \right|$ and $A_3 = \max_{(x,t) \in \Xi} \frac{1}{16} \left| \frac{\partial^{2n+2} w(x,t)}{\partial x^{n+1} \partial t^{n+1}} \right|$, gives

$$|w_n(x,t) - w(x,t)| \le A_1(\frac{L}{n})^{n+1} + A_2(\frac{S}{n})^{n+1} + A_3[\frac{(LS)^{\frac{1}{2}}}{n}]^{2n+2}. \tag{35}$$

So,

$$||w_n(x,t) - w(x,t)|| \le (LS)^{\frac{1}{2}} \left[A_1(\frac{L}{n})^{n+1} + A_2(\frac{S}{n})^{n+1} + A_3[\frac{(LS)^{\frac{1}{2}}}{n}]^{2n+2} \right]. \tag{36}$$

Similarly, considering $B_1 = \max_{(x,t) \in \Xi} \frac{1}{4} \left| \frac{\partial^{n+1} q(x,t)}{\partial x^{n+1}} \right|$, $B_2 = \max_{(x,t) \in \Xi} \frac{1}{4} \left| \frac{\partial^{n+1} q(x,t)}{\partial t^{n+1}} \right|$ and $B_3 = \max_{(x,t) \in \Xi} \frac{1}{16} \left| \frac{\partial^{2n+2} q(x,t)}{\partial x^{n+1} \partial t^{n+1}} \right|$, gives

$$|q_n(x,t) - q(x,t)| \le B_1(\frac{L}{n})^{n+1} + B_2(\frac{S}{n})^{n+1} + B_3[\frac{(LS)^{\frac{1}{2}}}{n}]^{2n+2}. \tag{37}$$

So,

$$||q_n(x,t) - q(x,t)|| \le (LS)^{\frac{1}{2}} \left[B_1(\frac{L}{n})^{n+1} + B_2(\frac{S}{n})^{n+1} + B_3[\frac{(LS)^{\frac{1}{2}}}{n}]^{2n+2} \right]. \tag{38}$$

The proof of Theorem 1 is completed. □

According to (35) and (36), the error bound of the absolute value form is $A_1(\frac{L}{n})^{n+1} + A_2(\frac{S}{n})^{n+1} + A_3[\frac{(LS)^{\frac{1}{2}}}{n}]^{2n+2}$ and the error bound of the space $L^2(\Xi)$ norm form is $(LS)^{\frac{1}{2}} \left[A_1(\frac{L}{n})^{n+1} + A_2(\frac{S}{n})^{n+1} + A_3[\frac{(LS)^{\frac{1}{2}}}{n}]^{2n+2} \right]$. In other words, $|w_n(x,t) - w(x,t)| \to 0$, $\forall (x,t) \in \Xi$ as $n \to \infty$. Also, $||w_n(x,t) - w(x,t)|| \to 0$, $\forall (x,t) \in \Xi$ as $n \to \infty$.

Once again, based on (37) and (38), the error bound of the absolute value form is $B_1(\frac{L}{n})^{n+1} + B_2(\frac{S}{n})^{n+1} + B_3[\frac{(LS)^{\frac{1}{2}}}{n}]^{2n+2}$ and the error bound of the space $L^2(\Xi)$ norm form is $(LS)^{\frac{1}{2}} \left[B_1(\frac{L}{n})^{n+1} + B_2(\frac{S}{n})^{n+1} + B_3[\frac{(LS)^{\frac{1}{2}}}{n}]^{2n+2} \right]$. In other words, $|q_n(x,t) - q(x,t)| \to 0$, $\forall (x,t) \in \Xi$ as $n \to \infty$. Also, $||q_n(x,t) - q(x,t)|| \to 0$, $\forall (x,t) \in \Xi$ as $n \to \infty$.

5 | NUMERICAL EXAMPLES

In this section, the numerical results obtained by the shifted Legendre polynomials algorithm are proposed on some test problems. The numerical example is chosen to show the efficiency and accuracy of the presented algorithm. A variable fractional order system of equations is considered, which contains an unknown piecewise analytical function. This numerical example

has the same form with the governing system of equations (4). The obtained solutions are compared with the exact solutions to establish the validity of the shifted Legendre polynomials algorithm.

To show the accuracy and efficiency , the absolute errors are expressed, using the following definitions:

$$\begin{cases} e_w(x, t) = |w_n(x, t) - w(x, t)| \\ e_q(x, t) = |q_n(x, t) - q(x, t)| \end{cases} \tag{39}$$

where $e_w(x, t)$ are absolute errors of numerical solutions $w_n(x, t)$ and exact solutions $w(x, t)$, $e_q(w, t)$ are absolute errors of numerical solutions $q_n(x, t)$ and exact solutions $q(x, t)$.

Example . Consider the following variable fractional order system of equations which is the same form as governing system of equations (4)

$$\begin{cases} \dfrac{\partial^2 w(x, t)}{\partial x^2} + \dfrac{\partial^2 w(x, t)}{\partial x \partial t} + \dfrac{\partial^2 w(x, t)}{\partial t^2} + \dfrac{\partial^{4+\alpha(x,t)} w(x, t)}{\partial x^4 \partial t^{\alpha(x,t)}} + \dfrac{\partial w(x, t)}{\partial t} + q(x, t) = f_1(x, t) \\ \dfrac{\partial^2 w(x, t)}{\partial t^2} + q(x, t) + \dfrac{\partial^2 q(x, t)}{\partial t^2} + \dfrac{\partial q(x, t)}{\partial t}(q^2(x, t) - 1) = f_2(x, t) \\ \alpha(x, t) = \begin{cases} 0.56 - 0.02(\dfrac{\partial^2 w(x, t)}{\partial x^2} - 0.01), & \dfrac{\partial^2 w(x, t)}{\partial x^2} \geq 0.01 \\ 0.56, & 0 \leq \dfrac{\partial^2 w(x, t)}{\partial x^2} < 0.01. \end{cases} \end{cases} \tag{40}$$

$\alpha(x, t)$ can be also equal to the following form

$$\alpha(x, t) = 0.56 - 0.01\left|\dfrac{\partial^2 w(x, t)}{\partial x^2} - 0.01\right| - 0.01(\dfrac{\partial^2 w(x, t)}{\partial x^2} - 0.01) \tag{41}$$

where

$$f_1(x, t) = t^2(12x^2 - 12x + 2) + 2t(4x^3 + 6x^2 + 2x) + 2(x^4 - 2x^3 + x^2)$$

$$+24\frac{\Gamma(3)}{\Gamma(3 - \alpha(x, t))}t^{2-\alpha(x,t)} + 2tx^2(1 - x)^2 + t^3 x(1 - x),$$

$$f_2(x, t) = 6tx(1 - x) + 2x^2(1 - x)^2 + t^3 x(1 - x) + 3t^8 x^3(1 - x)^3 - 3t^2 x(1 - x).$$

The exact solutions are expressed as:

$$\begin{cases} w(x, t) = x^2(1 - x)^2 t^2, & x \in [0, 1], t \in [0, 1] \\ q(x, t) = x(1 - x)t^3, & x \in [0, 1], t \in [0, 1]. \end{cases} \tag{42}$$

The boundary conditions are

$$\omega(0, t) = 0, \quad \omega(1, t) = 0, \quad \frac{\partial w(0, t)}{\partial x} = 0, \quad \frac{\partial w(1, t)}{\partial x} = 0. \tag{43}$$

TABLE 2 The exact solution and absolute error of Example 3 when x values 0.5 and n values 4.

	$t = 0.2$	$t = 0.4$	$t = 0.6$	$t = 0.8$	$t = 1.0$
$w(x, t)$	0.0025	0.0100	0.0225	0.0400	0.0625
$e_w(x, t)$	5.00×10^{-12}	3.84×10^{-12}	2.49×10^{-12}	0.30×10^{-12}	4.55×10^{-12}
$q(x, t)$	0.0020	0.0160	0.0540	0.1280	0.2500
$e_q(x, t)$	2.11×10^{-9}	1.73×10^{-9}	1.18×10^{-9}	0.46×10^{-9}	0.45×10^{-9}

The numerical example is a nonlinear variable fractional order system of equations which contains a cubic term of the analytic function. The numerical solutions $w_n(x, t)$ and $q_n(x, t)$ are obtained by shifted Legendre polynomials algorithm for n values 4. The absolute errors are shown in the first two figures in Fig. 2 . It shows that the absolute errors $e_w(x, t)$ and $e_q(x, t)$ are respectively less than 2×10^{-11} and 4×10^{-9}. In addition, the absolute error is far less than exact solution as shown in Table

(a) $e_w(x,t)$ (b) $e_q(x,t)$ (c) $\frac{\partial^2 w(x,t)}{\partial x^2}$
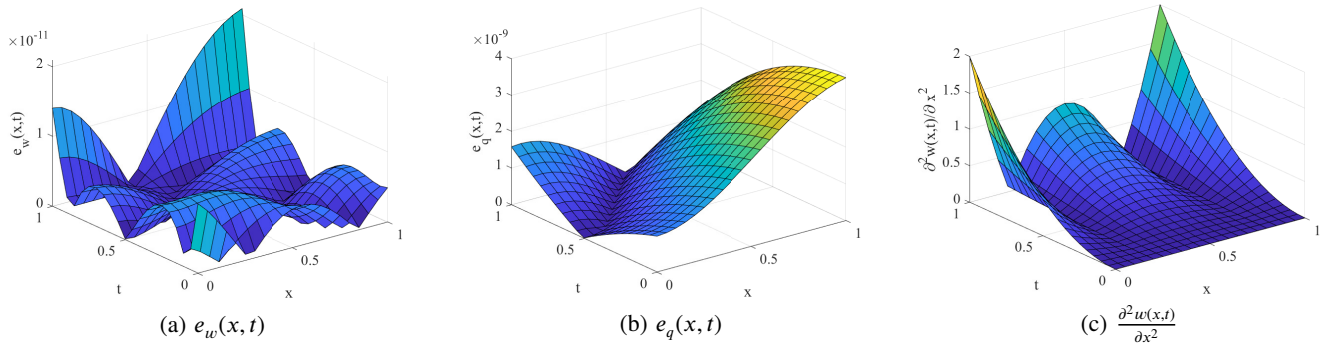
FIGURE 2 The absolute error and partial derivative $\frac{\partial^2 w(x,t)}{\partial x^2}$ of Example 3 when n values 4 for (a) $e_w(x,t)$, (b) $e_q(x,t)$ and (c) $\frac{\partial^2 w(x,t)}{\partial x^2}$.
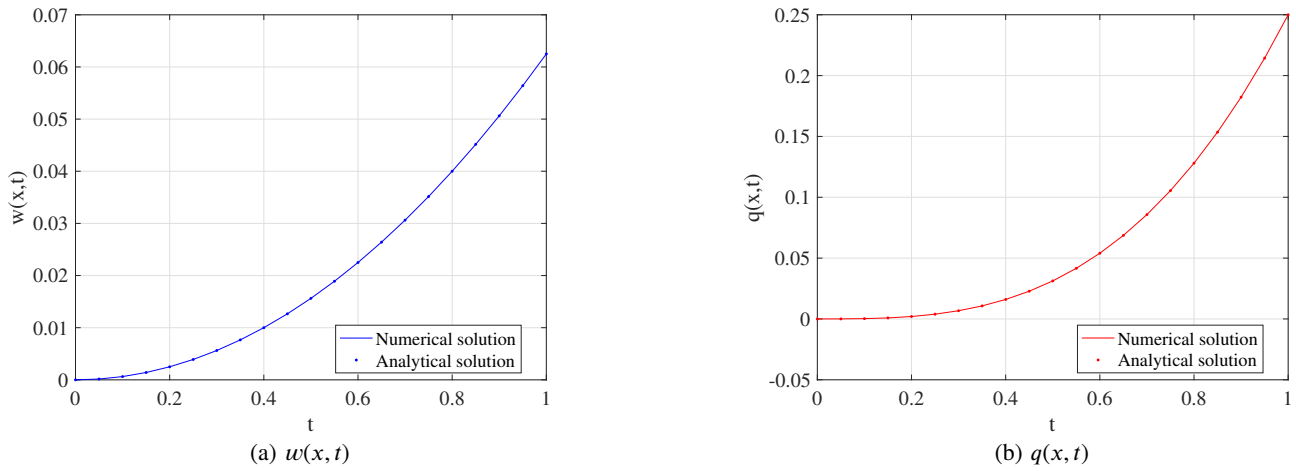

(a) $w(x,t)$ (b) $q(x,t)$

FIGURE 3 The numerical solution and exact solution of Example 3 when x values 0.5 and n values 4 for (a) $w(x,t)$ and (b) $q(x,t)$.

2 . The range of $\frac{\partial^2 w(x,t)}{\partial x^2}$ is in $[0,2]$ as shown in the third figure in Fig. 2 , which influences whether $\alpha(x,t)$ is a constant or an unknown piecewise function for analytical solution. Meanwhile, $\alpha(x,t)$ can also satisfy $0 < \alpha(x,t) < 1$. As can be seen from Fig. 3 , the numerical solution and exact solution of $w(x,t)$ and $q(x,t)$ are highly consistent. In all words, the above numerical results illustrate that shifted Legendre polynomials algorithm is accurate and effective for solving nonlinear variable fractional order system of equations, which is an unknown piecewise function.

6 | APPLICATION TO DYNAMIC ANALYSIS OF VISCOELASTIC PIPES

After the above validations, the shifted Legendre polynomials algorithm is applied to study practical vortex-induced vibration of viscoelastic pipes problems, which do not always have an exact solution. The influence of each parameter on viscoelastic pipe is analyzed. The feasibility of the proposed algorithm for solving practical problems is verified. In this section, the following non-dimensional quantities are introduced for making the governing system of equations (4) dimensionless:

$$y = \frac{w}{L}, \xi = \frac{x}{L}, \tau = \frac{t}{L}\sqrt{\frac{P_0}{m_f}}, \gamma = \sqrt{\frac{m_f}{P_0}},$$

$$\beta = \frac{m_f}{m}, q = \frac{EI}{P_0 L^2}\left(\frac{P_0}{m_f L^2}\right)^{\frac{\alpha}{2}}, \eta = \frac{C_s + \frac{1}{2}C_D \rho_0 DV_e}{\sqrt{Pm_f}},$$

$$k_L = \frac{C_D \rho_0 DV_e^2 m_f}{4mP_0}, k_e = \frac{m_f}{m_p}, \Omega_s = \frac{w_s}{L}\sqrt{\frac{P_0}{m_f}}.$$

Consequently, the nonlinear variable fractional order governing system of equations (4) can be transformed into the dimensionless forms as follows:

$$
\begin{cases}
\dfrac{\partial^2 y}{\partial \tau^2} + \beta \bigg\{ 2\gamma V_i \dfrac{\partial^2 y}{\partial \xi \partial \tau} + [\gamma^2 V_i^2 + \gamma \dfrac{\partial V_i}{\partial \tau}(1-\xi) - 1]\dfrac{\partial^2 y}{\partial \xi^2} \\
\qquad\qquad + \eta \dfrac{\partial y}{\partial \tau} + \varepsilon \theta^\alpha \dfrac{\partial^{4+\alpha} w}{\partial \xi^4 \partial \tau^\alpha} \bigg\} = k_L q + k_e f_e \\
\dfrac{\partial^2 q}{\partial \tau^2} + \lambda \Omega_s (q^2 - 1)\dfrac{\partial q}{\partial \tau} + \Omega_s^2 q = \dfrac{A_w}{D}\dfrac{\partial^2 y}{\partial \tau^2} \\
\alpha = \begin{cases}
\alpha_0 - \alpha_k \dfrac{D}{2}\dfrac{\partial^2 y}{\partial \xi^2}, & \dfrac{\partial^2 y}{\partial \xi^2} \geq \dfrac{2\alpha_b}{D} \\
\alpha_0, & 0 \leq \dfrac{\partial^2 y}{\partial \xi^2} < \dfrac{2\alpha_b}{D}.
\end{cases}
\end{cases}
\tag{44}
$$

TABLE 3 The fixed parameters in vortex-induced vibration of viscoelastic pipe conveying pulsating fluid.

Physical quantity	Symbol	Value	Dimension
Length of the pipe	L	100	m
Outer diameter of the pipe	D	0.5	m
Inner diameter of the pipe	d	0.3	m
Area moment of inertia	I	0.0027	m^4
Constitutive model parameter	E	100	GPa
Constitutive model parameter	θ	0.01	1
Density of external fluid	ρ_0	1020	$\text{kg} \cdot \text{m}^{-3}$
Tensional force	P_0	1000	N
Internal damping coefficient	C_s	50	$\text{N} \cdot \text{s} \cdot \text{m}^{-2}$

Dynamic response of the viscoelastic pipe undergoing vortex-induced vibration and conveying pulsating fluid is analyzed with the above form of governing system of equations. Numerical results are obtained by shifted Legendre polynomials algorithm for n selected as 4. Moreover, the ring-shaped pipe is considered, and the fixed parameters are listed in Table 3 .

Here external fluid velocity V_e, internal fluid velocity V_i, density ρ_f and force excitation f_e are expressed as the following form

$$V_e = V_0(1 - \xi) \tag{45}$$

where V_e is varying with the deep of the pipe, V_0 is the external fluid velocity at the top of pipe.

$$V_i = V_{ib} + V_{is}\sin(\omega_{V_i}\tau) \tag{46}$$

where V_{ib}, V_{is} and ω_{V_i} are respectively the basic velocity, fluctuation velocity and fluctuation frequency of the internal fluid.

$$\rho_f = \rho_{f_b} + \rho_{f_k}\tau \tag{47}$$

where ρ_{f_b} and ρ_{f_k} are respectively the basic density and varying rate of the internal fluid.

$$f_e = f_{e_b} + f_{e_s}\sin(f_{e_\omega}\tau) \tag{48}$$

where f_{e_b}, f_{e_s} and f_{e_ω} are respectively the basic force, fluctuation force and fluctuation frequency of the force excitation.

Meanwhile, three physical quantities non-dimensional displacement $y(\xi,\tau)$, non-dimensional velocity $v(\xi,\tau)$ and non-dimensional acceleration $a(\xi,\tau)$ of the pipe are used for the dynamic analysis. $v(\xi,\tau)$ and $a(\xi,\tau)$ are expressed as the following form:

$$v(\xi,\tau) = \frac{\partial y(\xi,\tau)}{\partial \tau}; \quad a(\xi,\tau) = \frac{\partial^2 y(\xi,\tau)}{\partial \tau^2}. \tag{49}$$
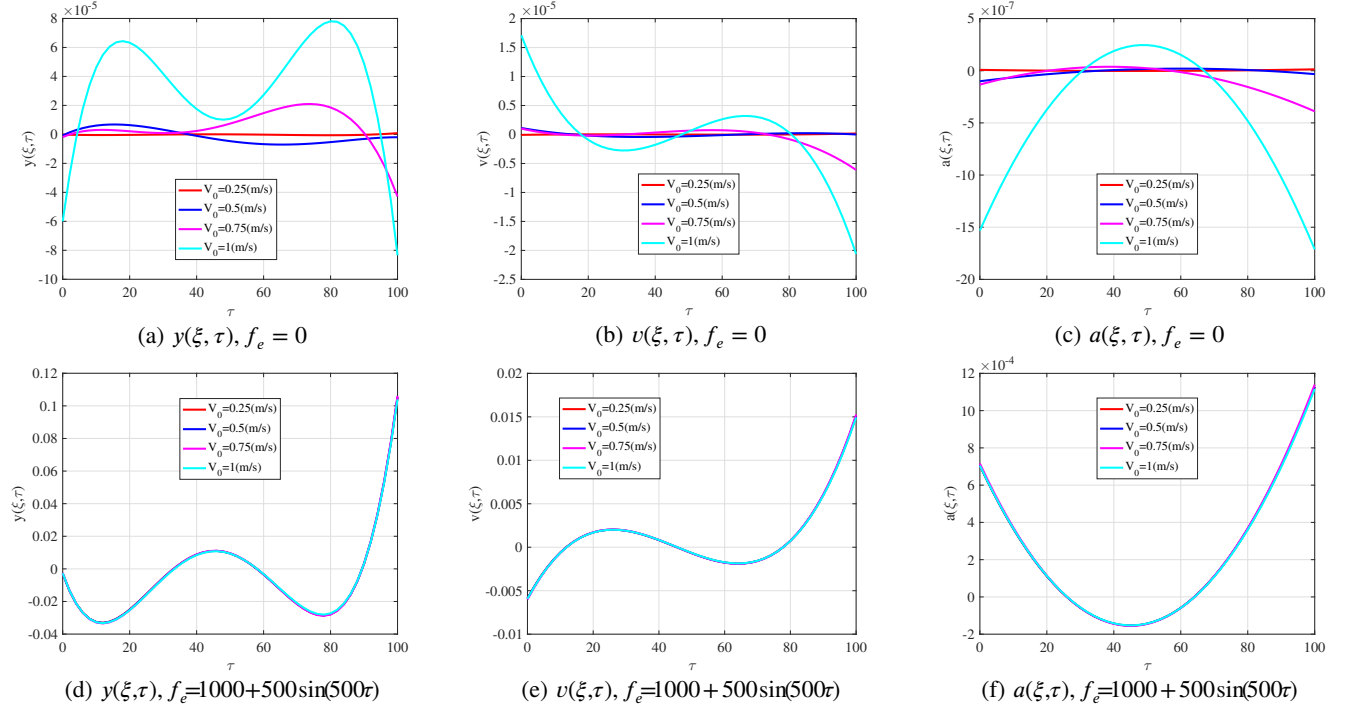

(a) $y(\xi,\tau)$, $f_e = 0$ (b) $v(\xi,\tau)$, $f_e = 0$ (c) $a(\xi,\tau)$, $f_e = 0$

(d) $y(\xi,\tau)$, $f_e=1000+500\sin(500\tau)$ (e) $v(\xi,\tau)$, $f_e=1000+500\sin(500\tau)$ (f) $a(\xi,\tau)$, $f_e=1000+500\sin(500\tau)$

FIGURE 4 Dynamic analysis of viscoelastic pipe conveying fluid when n values 4 for (a) $y(\xi,\tau)$, $f_e = 0$, (b) $v(\xi,\tau)$, $f_e = 0$, (c) $a(\xi,\tau)$, $f_e = 0$, (d) $y(\xi,\tau)$, $f_e = 1000 + 500\sin(500\tau)$, (e) $v(\xi,\tau)$, $f_e = 1000 + 500\sin(500\tau)$ and (f) $a(\xi,\tau)$, $f_e = 1000 + 500\sin(500\tau)$.

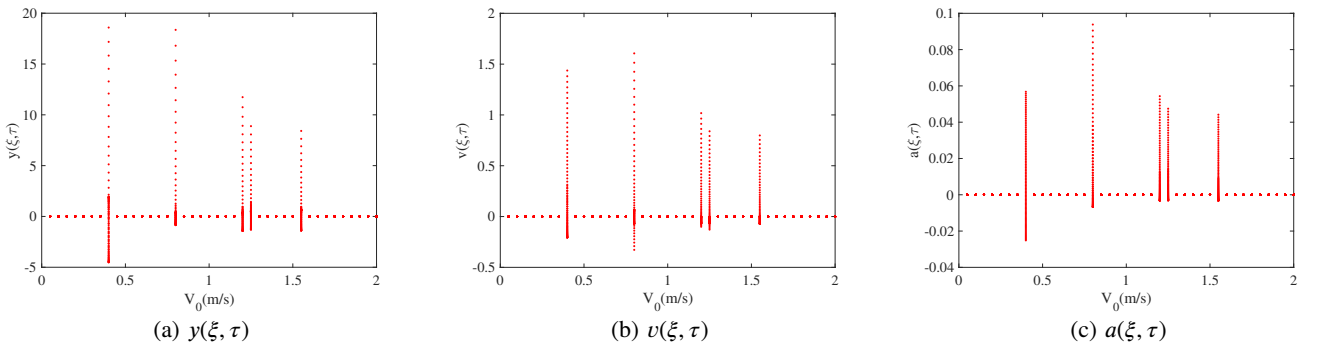(a) $y(\xi,\tau)$ (b) $v(\xi,\tau)$ (c) $a(\xi,\tau)$

FIGURE 5 Bifurcation diagram as V_0 varying when n values 4 for (a) $y(\xi,\tau)$, (b) $v(\xi,\tau)$ and (c) $a(\xi,\tau)$.

Firstly, the influence of external fluid velocity on the dynamic response of the pipe is analyzed when the external force excitation is determined. As shown in the first three figures in Fig. 4 , When the external excitation $f_e = 0$, the external fluid velocity increases, so does the displacement, velocity and acceleration of the pipe. But, when $f_e = 1000 + 500\sin(500\tau)$ in the

last three figures in Fig. 4 , displacement, velocity and acceleration are no significant change. Therefore, This illustrates that external force excitation can attenuate the effect of external fluid velocity on the pipe.

The following analysis is the effect of various factors on the chaotic state of the pipe.

The first factor is external fluid velocity $V_e = V_0(1-\xi)$, the value of V_0 in Fig. 5 ranges from 0 to 2 m/s. When V_0 takes several fixed values, the displacement, velocity and acceleration of the pipe will enter an instant chaotic state.
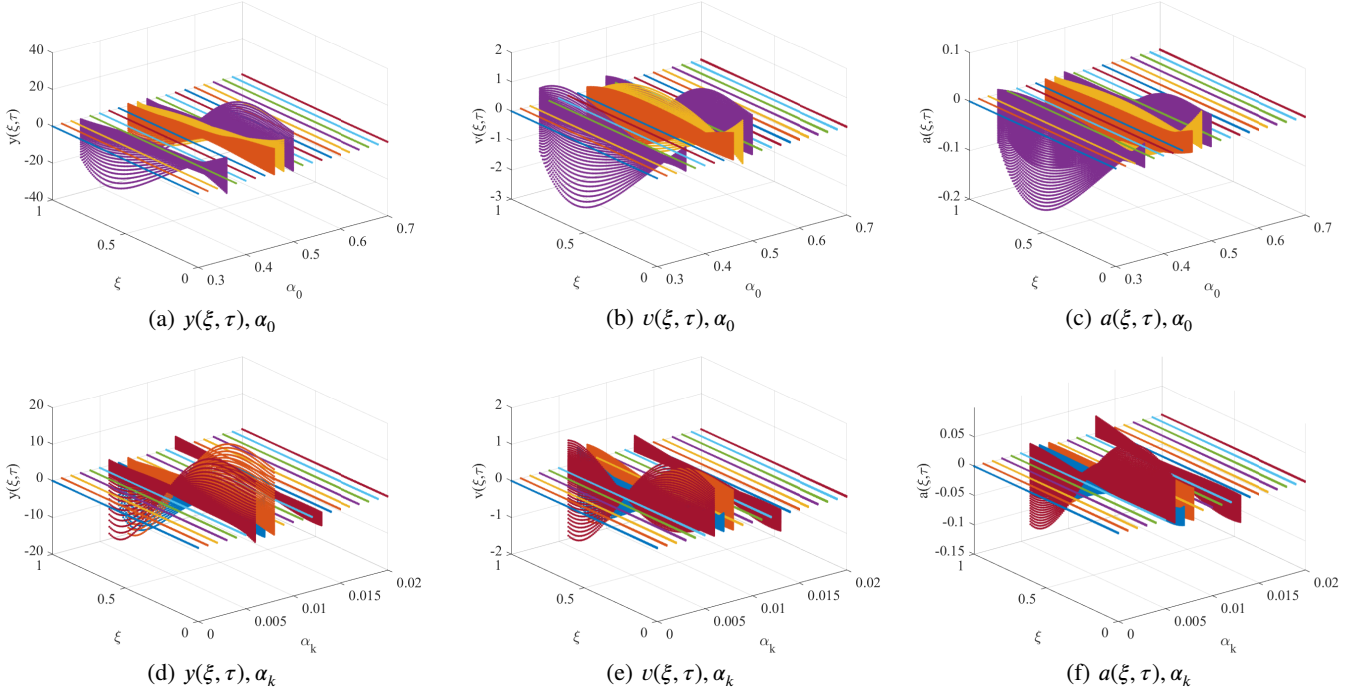

FIGURE 6 Three-dimensional dynamic response map as α varying when n values 4 for (a) $y(\xi,\tau),\alpha_0$, (b) $v(\xi,\tau),\alpha_0$, (c) $a(\xi,\tau),\alpha_0$, (d) $y(\xi,\tau),\alpha_k$, (e) $v(\xi,\tau),\alpha_k$ and (f) $a(\xi,\tau),\alpha_k$.

The second factor is variable fractional order $\alpha = \alpha_0 - \alpha_k \dfrac{D}{2}\dfrac{\partial^2 y}{\partial \xi^2}$, when $\dfrac{\partial^2 y}{\partial \xi^2} \geq \dfrac{2\alpha_b}{D}$. With the change of α_0 in the first three figures in Fig. 6 , when α_0 takes several fixed values, the displacement, velocity and acceleration of the pipe will enter an instant chaotic state. Similarly, when α_k takes several fixed values in the last three figures in Fig. 6 ,the displacement, velocity and acceleration of the pipe will also enter an instant chaotic state.
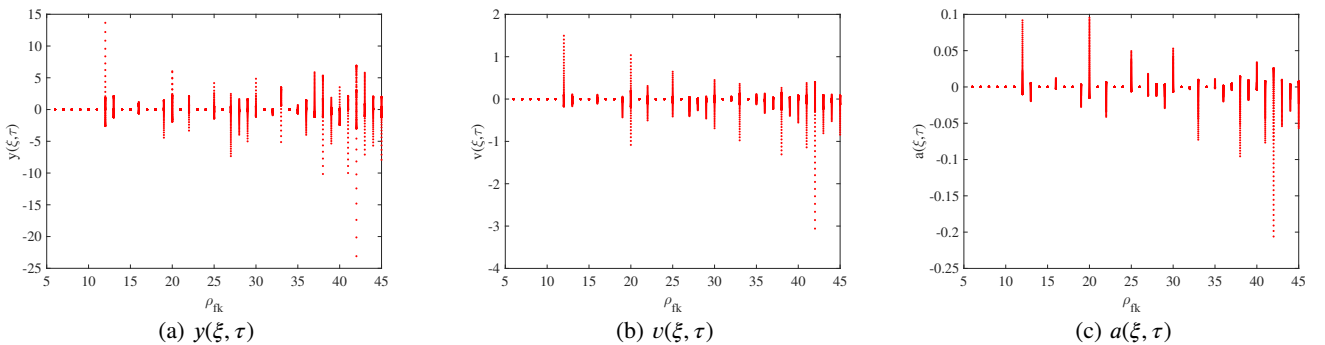

FIGURE 7 Dynamic response as ρ_{f_k} varying when n values 4 for (a) $y(\xi,\tau)$, (b) $v(\xi,\tau)$ and (c) $a(\xi,\tau)$.

The third factor is the internal fluid density $\rho_f = \rho_{f_b} + \rho_{f_k}\tau$ in Fig. 7 , With the increase of ρ_{f_k}, the displacement, velocity and acceleration of the pipe enter into a long-term chaotic state.

The viscoelastic pipe would occur to be a strong oscillation response at chaotic state. Meanwhile, this can cause the viscoelastic pipe damaged and bring unpredictable losses. According to the above analysis and discussions, the physical quantity values and value regions of the viscoelastic pipe entering chaotic state can be computed by the shifted Legendre polynomials algorithm at different cases. The proposed algorithm contributes to the physics and sciences field related to vortex-induced vibration of the viscoelastic pipe conveying fluid and avoids risk physical quantity values and value regions. The shifted Legendre polynomials algorithm provides a guarantee for the safe and effective performance of the viscoelastic pipe.

7 | CONCLUSIONS

Due to the lack of research on fluid-solid coupling variable fractional nonlinear dynamics, the vortex-induced vibration dynamics of viscoelastic pipes conveying pulsating fluid is studied based on the variable fractional order model. A class of nonlinear variable fractional order composed of unknown piecewise analytic function system of equations is established. And the analytic model of vortex-induced vibration problem is more accurate than ever. The shifted Legendre polynomials algorithm is proposed for solving this kind of system of equations. At the same time, it is verified that the proposed numerical algorithm is accurate and efficient for this kind of problems by convergence analysis and numerical examples. From the numerical results obtained by the proposed algorithm, the following conclusions are drawn:

1. When the force excitation values 0, the dynamic response of the viscoelastic pipes increases nonlinearly with the linear variation of the external fluid velocity. However, when the force excitation value is large, the effect of external fluid velocity on the dynamic response is almost zero.

2. In the problem of vortex-induced vibration of viscoelastic pipes conveying pulsating fluid, the dynamic response will change and enter the chaotic state with the change of parameters. The displacement, velocity and acceleration of the pipe will enter an transcient chaotic state with external fluid velocity and variable fractional order reaching several certain values. The displacement, velocity and acceleration of the pipe will enter a long-term chaotic state with density of internal pulsating fluid being in a certain value region.

3. The shifted Legendre polynomials algorithm contributes to the viscoelastic pipe for avoiding risk physical quantity values and value regions due to great potential for high-precision problems. Furthermore, the proposed algorithm not only plays a theoretical foundation for the engineering field, but also has a guiding significance for further research in physics and science.

AUTHOR CONTRIBUTIONS

All authors read and approved the final manuscript.

CONFLICT OF INTEREST

The authors declare that there is no conflict of interests regarding the publication of this article.

ORCID

Yiming Chen https://orcid.org/0000-0001-7040-8050

References

1. Yun KS, Youn SK. Microstructural topology optimization of viscoelastic materials of damped structures subjected to dynamic loads. *Int J Solids Struct*. 2018;147:67−79. DOI:10.1016/j.ijsolstr.2018.04.022.

2. Mohammad HS, Abbas R, Saeed Z. Predictions of viscoelastic behavior of pomegranate using artificial neural network and Maxwell model. *Comput Electron Agr*. 2013;98:1−7. DOI:10.1016/j.compag.2013.07.009

3. Yan W, Ying J, Chen WQ. The behavior of angle-ply laminated cylindrical shells with viscoelastic interfaces in cylindrical bending. *Compos Struct*. 2007;78(4):551−559. DOI:10.1016/j.compstruct.2005.11.017.

4. Abobakr A, Said LA, Madian AH, Elwakil AS, Radwan AG. Experimental Comparison of Integer/Fractional-order Electrical Models of Plant. *Int J Electron Commun*. 2017;80:1−9. DOI:10.1016/j.aeue.2017.06.010.

5. Yu CX, Zhang J, Chen YM, Feng YJ, Yang AM. A numerical method for solving fractional-order viscoelastic Euler-Bernoulli beams. *Chaos Solitons Fract*. 2019;128:275−279. DOI:10.1016/j.chaos.2019.07.035.

6. Martin O. Nonlocal effects on the dynamic analysis of a viscoelastic nanobeam using a fractional Zener model. *Appl Math Model*. 2019;73:637−650. DOI:10.1016/j.apm.2019.04.029.

7. Yin YB, Zhu KQ. Oscillating flow of a viscoelastic fluid in a pipe with the fractional Maxwell model. *Appl Math Comput*. 2006;173:231−242. DOI:10.1016/j.amc.2005.04.001.

8. Sweilam NH, AL-Mekhlafi SM, Albalawi AO, Machado JAT. Optimal control of variable-order fractional model for delay cancer treatments. *Appl Math Model*. 2021;89:1557−1574. DOI:10.1016/j.apm.2020.08.012.

9. Li Z, Wang H, Xiao R, Yang S. A variable-order fractional differential equation model of shape memory polymers. *Chaos Solitons Fract*. 2017;102:473−485. DOI:10.1016/j.chaos.2017.04.042.

10. Meng RF, Yin DS, Drapaca CS. Variable-order fractional description of compression deformation of amorphous glassy polymers. *Comput Mech*. 2019;64:163−171. DOI:10.1007/s00466-018-1663-9.

11. Cai W, Wang P, Fan JJ. A variable-order fractional model of tensile and shear behaviors for sintered nano-silver paste used in high power electronics. *Mech Mater*. 2020;145:103391. DOI:10.1016/j.mechmat.2020.103391.

12. Meng RF, Yin DS, Yang HX, Xiang GJ. Parameter study of variable order fractional model for the strain hardening behavior of glassy polymers. *Phys A:Sta Mech Appl*. 2020;545:123763. DOI:10.1016/j.physa.2019.123763.

13. Zheng HX, wang JS. A numerical study on the vortex-induced vibration of flexible cylinders covered with differently placed buoyancy modules. *J Fluids Struct*. 2021;100:103174. DOI:10.1016/j.jfluidstructs.2020.103174.

14. Dai HL, Wang L, Qian Q, Ni Q. Vortex-induced vibrations of pipes conveying fluid in the subcritical and supercritical regimes. *J Fluids Struct*.2013;39(5):322−334. DOI:10.1016/j.jfluidstructs.2013.02.015.

15. Duan JL, Chen K, You YX, Wang RF, Li JL. Three-dimensional dynamics of vortex-induced vibration of a pipe with internal flow in the subcritical and supercritical regimes. *Int J Naval Arch Ocean Eng*. 2018;10(6):692−710. DOI:10.1016/j.ijnaoe.2017.11.002.

16. Xie WD, Gao XF, Wang EH, Xu WH, Bai YC. An investigation of the nonlinear dynamic response of a flexible pipe undergoing vortex-induced vibrations and conveying internal fluid with variable-density. *Ocean Eng*. 2019;183:453−468. DOI:10.1016/j.oceaneng.2019.05.005.

17. Dai HL, Wang L, Qian Q, Ni Q. Vortex-induced vibrations of pipes conveying pulsating fluid. *Ocean Eng*. 2014;77:12−22. DOI:10.1016/j.oceaneng.2013.12.006.

18. Yang WW, Ai ZJ, Zhang XD, Chang XP, Gou RY. Nonlinear dynamics of three-dimensional vortex-induced vibration prediction model for a flexible fluid-conveying pipe. *Int J Mech Sci*. 2018;138-139:99−109. DOI:10.1016/j.ijmecsci.2018.02.005.

19. Zhang XD, Gou RY,Yang WW, Chang XP. Vortex-induced vibration dynamics of a flexible fluid-conveying marine riser subjected to axial harmonic tension. *J Brazil Soc Mech Sci Eng*. 2018;40(8):365. DOI:10.1007/s40430-018-1289-z.

20. Keramat A, Tijsseling AS, Hou Q, Ahmadi A. Fluid-structure interaction with pipe-wall viscoelasticity during water hammer. *J Fluids Struct*. 2012;28(1):434−455. DOI:10.1016/j.jfluidstructs.2011.11.001.

21. Wahba EM. On the two-dimensional characteristics of laminar fluid transients in viscoelastic pipes. *J Fluids Struct*. 2017;68:113−124. DOI:10.1016/j.jfluidstructs.2016.10.012.

22. Yang WW, Ai ZJ, Zhang XD, Gou RY, Chang XP. Nonlinear three-dimensional dynamics of a marine viscoelastic riser subjected to uniform flow. *Ocean Eng*. 2018;149:38−52. DOI:10.1016/j.oceaneng.2017.12.004.

23. Qu HD, Liu X, She Z. Neural network method for fractional-order partial differential equations. *Neurocomputing*. 2020;414:225−237. DOI:10.1016/j.neucom.2020.07.063.

24. Ramezani M. Numerical analysis nonlinear multi-term time fractional differential equation with collocation method via fractional B-spline. *Math Meth Appl Sci*. 2019;42(1):4640−4663. DOI:10.1002/mma.5642.

25. Ansari A, Sheikhani AR, Najafi HS. Solution to system of partial fractional differential equations using the fractional exponential operators. *Math Meth Appl Sci*. 2012;35(1):119−123. DOI:10.1002/mma.1545.

26. Chen YM , Wei YQ, Liu DY, Boutat D, Chen XK. Variable-order fractional numerical differentiation for noisy signals by wavelet denoising. *J Comput Phys*. 2016;311:338−347. DOI:10.1016/j.jcp.2016.02.013.

27. El-Sayed AA, Agarwal P. Numerical solution of multiterm variable-order fractional differential equations via shifted Legendre polynomials. *Math Meth Appl Sci*. 2019;42(11):3978−3991. DOI:10.1002/mma.5627.

28. Chen YM, Liu LQ, Li BF, Sun YN. Numerical solution for the variable order linear cable equation with Bernstein polynomials. *Appl Math Comput*.2014;238:329−341. DOI:10.1016/j.amc.2014.03.066.

29. Tayebi A, Shekari Y, Heydari MH. A meshless method for solving two-dimensional variable-order time fractional advection-diffusion equation. *J Comput Phys*. 2017;340:655−669. DOI:10.1016/j.jcp.2017.03.061.

30. Liu JM, Li XK, Hu XL. A RBF-based differential quadrature method for solving two-dimensional variable-order time fractional advection-diffusion equation. *J Comput Phys*. 2019;384:222−238. DOI:10.1016/j.jcp.2018.12.043.

31. Faghih A, Mokhtary P. A new fractional collocation method for a system of multi-order fractional differential equations with variable coefficients. *J Comput Appl Math*. 2021;383:113139. DOI:10.1016/j.cam.2020.113139.

32. Heydari MH, Avazzadeh Z, Atangana A. Orthonormal shifted discrete Legendre polynomials for solving a coupled system of nonlinear variable-order time fractional reaction-advection-diffusion equations. *Appl Num Math*. 2021;161:425−436. DOI:10.1016/j.apnum.2020.11.020.

33. Coimbra CFM. Mechanics with variable-order differential operators. *Annalen der Physik*. 2003;12(11-12):692−703. DOI:10.1002/andp.200310032.

34. Meng RF, Yin DS, Drapaca CS. A variable order fractional constitutive model of the viscoelastic behavior of polymers. *Int J Non-Linear Mech*. 2019;113:171−177. DOI:10.1016/j.ijnonlinmec.2019.04.002.

35. Chen YM, Ke XH, Wei YQ. Numerical algorithm to solve system of nonlinear fractional differential equations based on wavelets method and the error analysis. *Appl Math Comput*. 2015;143:203−222. DOI:10.1016/j.amc.2014.11.079

APPENDIX

A THE DERIVATION PROCESS OF THE GOVERNING SYSTEM OF EQUATIONS OF VISCOELASTIC PIPES CONVEYING FLUID

This section illustrates the specific derivation process of Eq.(4). It is noted that the physical quantities not specifically explained in this section are given in Table 1 .

Hamilton's principal is written as the following form:

$$\int_{t_1}^{t_2} (\delta T - \delta V + \delta W) dt = 0 \tag{A1}$$

where T is total kinetic energy, V is potential energy, W is nonconservative work.

Total kinetic energy T contains three parts

$$T = T_p + T_f + T_a \tag{A2}$$

where the kinetic energy of the pipe $T_p = \frac{1}{2} m_p \int_0^L (\frac{\partial w}{\partial t})^2 dx$, the kinetic energy of the internal fluid $T_f = \frac{1}{2} m_f \int_0^L \left[(\frac{\partial w}{\partial t} + V_i \frac{\partial w}{\partial x})^2 + V_i^2 \right] dx$ and the kinetic energy of the additional external fluid $T_a = \frac{1}{2} m_a \int_0^L (\frac{\partial w}{\partial t})^2 dx$. Similarly, total mass per unit length contains three parts $m = m_p + m_f + m_a$ where m_p is mass per unit length of the pipe, m_f is mass per unit length of the internal fluid and m_a is mass per unit length of the additional external fluid which is defined as $m_a = \frac{1}{4} \pi \rho_0 D^2$.

The potential energy of the pipe is written as:

$$V = \frac{1}{2} \int_{V_r} \left[E\theta^\alpha (-z \frac{\partial^{2+\alpha} w}{\partial x^2 \partial t^\alpha}) - P_0 \right] \varepsilon dV_r \tag{A3}$$

where $\varepsilon = -z \frac{\partial^2 w}{\partial x^2}$, z is the radial coordinate of the circular section for the pipe and V_r is the volume of the pipe.

The nonconservative work W is formulated as:

$$\delta W = \int_0^L f \delta w dx - \int_0^L C_s \frac{\partial w}{\partial t} \delta w dx \tag{A4}$$

where f is the vortex-induced and excitation forces.

Substituting Eqs.(A2)-(A4) into Eq.(A1) respectively, the following formulations hold:

$$m \frac{\partial^2 w}{\partial t^2} + [m_f V_i^2 + m_f \frac{\partial V_i}{\partial t}(L - x) - P_0] \frac{\partial^2 w}{\partial x^2}$$

$$+ 2 m_f V_i \frac{\partial^2 w}{\partial x \partial t} + E I \theta^\alpha \frac{\partial^{4+\alpha} w}{\partial x^4 \partial t^\alpha} + C_s \frac{\partial w}{\partial t} = f. \tag{A5}$$

In addition, force f containing three parts hydrodynamic damping force $f_D(x,t) = -\frac{1}{2} C_D \rho_0 D V_e \frac{\partial w}{\partial t}$, lift force $f_L(x,t) = \frac{1}{4} C_{L_0} \rho_0 D V_e^2 q$ and excitation force f_e can be expressed as:

$$f = f_D + f_L + f_e \tag{A6}$$

Furthermore, the second formulation of Eq.(4) is from Ref.[14] and the third formulation of Eq.(4) is from Ref.[34]. After the above derivation, the governing system of equations are written as Eq.(4).